Tunable Mode Coupling in Nanocontact Spin-Torque Oscillators

Steven S.-L. Zhang,[1,2,*] Ezio Iacocca,[3,4] and Olle Heinonen[2,5,6,†]

[1]*Department of Physics and Astronomy, University of Missouri, Columbia, Missouri 65211, USA*
[2]*Material Science Division, Argonne National Laboratory, Lemont, Illinois 60439, USA*
[3]*Department of Applied Mathematics, University of Colorado, Boulder, Colorado 80309-0526, USA*
[4]*Department of Physics, Division for Theoretical Physics, Chalmers University of Technology, 412 96 Gothenburg, Sweden*
[5]*Northwestern-Argonne Institute of Science and Technology, 2145 Sheridan Road, Evanston, Illinois 60208, USA*
[6]*Computation Institute, The University of Chicago, 5735 South Ellis Avenue, Chicago, Illinois 60637, USA*
(Received 10 April 2017; revised manuscript received 27 June 2017; published 27 July 2017)

Recent experiments on spin-torque oscillators have revealed interactions between multiple magnetodynamic modes, including mode coexistence, mode hopping, and temperature-driven crossover between modes. The initial multimode theory indicates that a linear coupling between several dominant modes, arising from the interaction of the subdynamic system with a magnon bath, plays an essential role in the generation of various multimode behaviors, such as mode hopping and mode coexistence. In this work, we derive a set of rate equations to describe the dynamics of coupled magnetodynamic modes in a nanocontact spin-torque oscillator. Expressions for both linear and nonlinear coupling terms are obtained, which allow us to analyze the dependence of the coupled dynamic behaviors of modes on external experimental conditions as well as intrinsic magnetic properties. For a minimal two-mode system, we further map the energy and phase difference of the two modes onto a two-dimensional phase space and demonstrate in the phase portraits how the manifolds of periodic orbits and fixed points vary with an external magnetic field as well as with the temperature.

DOI: 10.1103/PhysRevApplied.8.014034

I. INTRODUCTION

Since the discovery of the spin-transfer-torque (STT) effect [1,2], efficient manipulation of the magnetization orientation can be achieved by applying a dc current perpendicularly to a magnetic heterostructure consisting of two magnetic layers separated by a nonmagnetic spacer. The current becomes spin polarized when passing through the magnetic layer with a fixed magnetization direction and subsequently transfers spin angular momentum to the other magnetic layer by exerting a spin torque on the magnetization. One particularly important manifestation of the STT effect is the steady-state magnetization dynamics at microwave frequencies that is realized in devices known as spin-torque oscillators (STOs) [3,4]. These are typically fabricated in either nanopillar or nanocontact (NC) geometry and rely on the compensation of intrinsic damping by STT as the current approaches a threshold for auto-oscillations. With the appropriate arrangement of the relative orientations of the magnetizations as well as of the current direction, nearly undamped oscillation modes with a very small linewidth can be realized in STOs.

As an attempt to describe the magnetodynamics in STOs, Slavin and co-workers [5] developed a single-mode theory under the assumption that only a single coherent precessional mode is excited, which captures some remarkable nonlinear features of STOs qualitatively and to some extent quantitatively. The assumption of single-mode precession further precludes chaos and the possibility of mode transitions between dynamical modes [6]. Later, an effective theory of a two-mode STO was put forth by de Aguiar, Azevedo, and Rezende [7]. By solving the equations of motion for the amplitudes of the two modes, nonlinearly coupled by third-order terms originating from four-magnon interactions, they conclude that, in the steady state, only one mode will survive whereas the other will be extinguished. However, neither of these theories mentioned above can explain recent experimental observations of a variety of multimode dynamical effects in STOs such as mode hopping [8–10], periodic mode transitions [11,12], and mode coexistence [13,14]. In addition to mode hopping, Muduli, Heinonen, and Åkerman [10] also note a mode crossover driven by the *temperature* with other parameters, such as the current and external magnetic field, kept fixed. Clearly, such temperature-driven behavior points to a highly nontrivial temperature dependence which must be explained by more comprehensive theories.

A multimode theory was proposed by Muduli, Heinonen, and Åkerman [9] to explain the observed mode hopping in nanopillar STOs. The authors show,

*shulei.zhang@anl.gov
†heinonen@anl.gov

for a minimal two-mode system, that the rate equations for the slowly varying mode amplitudes can be mapped onto a two-dimensional Z_2-symmetric dynamical system, in analogy with those for two counterpropagating modes in semiconductor ring lasers [15,16]. A key ingredient of the theory is the assumption that there exists, in addition to third-order nonlinear coupling terms [7], a linear coupling between the modes, which is essential for the mode hopping to occur. By treating the various coupling coefficients in the rate equations as phenomenological parameters, the effective multimode theory has been well substantiated by later experimental observations that are related to mode hopping, including linewidth broadening in NC STOs [17] and a $1/f$-frequency noise spectrum in STOs [18,19].

Effective control of STOs, however, requires an in-depth understanding of the underlying physics of the mode coupling. For this purpose, the multimode theory was derived rigorously [20] from the micromagnetic Landau-Lifshitz-Gilbert equation, whereby the crucial linear coupling term is shown to arise from the interaction of a dynamical subsystem, which involves several dominant modes, with a thermal bath of magnons. This theoretical assertion is consistent with the two kinds of mode-coupling mechanisms that are identified experimentally in NC STOs by Iacocca *et al.* [14], namely, magnon-mediated scattering and intermode interaction. In this paper, we apply the multimode theory to a NC STO for which approximate analytic profiles of the eigenmodes are available [21] and, hence, simplified expressions for both linear and nonlinear coupling terms can be derived explicitly. With these expressions, we further determine the dependence of the mode coupling and the ensuing dynamics of the STO on typical controllable experimental parameters such as the external magnetic field and temperature.

The remainder of the paper is organized as follows. In Sec. II, we outline the derivation of the coupled rate equations for the two lowest-lying eigenmodes of a NC STO, where the linear coupling term appears after the thermal bath of magnons is integrated out and the equations are projected onto the subspace of the two modes. We present explicitly the expressions for both linear and nonlinear coupling terms and, in particular, show the dependence of the linear coupling term on the external magnetic field and temperature. We also reveal the correlation between the linear coupling and the nonlinear spin-wave frequency shift. In Sec. III, we transform the rate equations to a more appealing form, which allows the mapping of the energy and phase difference of the two modes onto a two-dimensional phase space. We show in the resulting phase portraits how the manifolds of periodic orbits and fixed points, both stable and unstable ones, vary with an external magnetic field as well as the temperature. Finally, we discuss and summarize our results in Sec. IV.

II. MODE EQUATIONS WITH LINEAR COUPLING

We consider a NC STO based on a pseudospin valve composed of ferromagnetic (FM) fixed and free layers separated by a metallic nonmagnetic (NM) spacer, as shown in Fig. 1. We further assume that the pseudospin valve is patterned into a disk of radius R_F. A nanocontact of radius R_c is defined on top of the free layer such that $R_c \ll R_F$. This configuration allows a current to flow through a cylindrical region directly below the nanocontact, which has been shown to be in good agreement with experiments [4].

The magnetization dynamics in a nanocontact spin-torque oscillator can be described by the generalized Landau-Lifshitz equation with current-induced spin-transfer torque [1,2], i.e.,

$$\frac{\partial \mathbf{m}}{\partial t} = -\gamma \mathbf{m} \times \mathbf{H}_{\rm eff} - \frac{\gamma\alpha}{1+\alpha^2}\mathbf{m} \times (\mathbf{m} \times \mathbf{H}_{\rm eff}) + \gamma a_J(r)\mathbf{m} \times (\mathbf{m} \times \hat{\mathbf{M}}_p), \tag{1}$$

where γ is the gyromagnetic ratio, α is the dimensionless Gilbert damping parameter, and $\mathbf{m}$ and $\hat{\mathbf{M}}_p$ are the unit vectors denoting the local magnetization direction of the free layer and the uniform magnetization direction of the fixed layer, respectively. The strength of the STT is characterized by an effective field $a_J(r) = a_J\mathcal{H}(R_c - r)$ with $\mathcal{H}(R_c - r)$ the Heaviside step function describing the confinement of the current in the NC STO within a cylindrical region of radius R_c. The total effective magnetic field $\mathbf{H}_{\rm eff}$ is taken to be a superposition of the external field, the anisotropy field, the exchange field, and the demagnetization field, which can be expressed as

$$\mathbf{H}_{\rm eff} = \mathbf{H}_{\rm ext} + H_a m_x \boldsymbol{e}_x + (2A_{\rm ex}/M_s)\nabla^2\mathbf{m} - 4\pi M_s m_z \boldsymbol{e}_z,$$

where $\mathbf{H}_{\rm ext}$ is the uniform external field, H_a is the magnitude of the anisotropy field, $A_{\rm ex}$ is the exchange

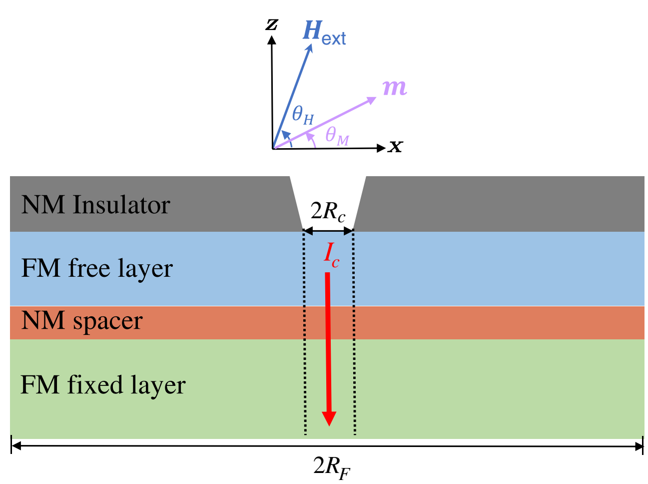

FIG. 1. Schematic diagram of the side view of a nanocontact spin-torque oscillator.

stiffness, and the perpendicular-to-plane demagnetization field is reduced to the local form in the zero-thickness limit or thin-film approximation. To simplify our discussion, we restrict ourselves to a simple geometry where the magnetization of the fixed layer is lying along the x axis [22], i.e., $\hat{\mathbf{M}}_p = \boldsymbol{e}_x$, and both the magnetization of the free layer and the external magnetic field are varied within the x-z plane, i.e., $\mathbf{m} = \cos\theta_M \boldsymbol{e}_x + \sin\theta_M \boldsymbol{e}_z$ and $\mathbf{H}_{\rm ext} = H_{\rm ext}(\cos\theta_H \boldsymbol{e}_x + \sin\theta_H \boldsymbol{e}_z)$.

At temperatures well below the Curie temperature, it is a good approximation to assume that the magnitude of the free-layer magnetization $\mathbf{m}$ is conserved [as implied by Eq. (1)]. This leaves only two independent components of $\mathbf{m}$, which can be expressed in terms of a single (space-dependent) complex spin-wave variable $a(\mathbf{r}) = a[\mathbf{m}(\mathbf{r})]$, characterizing the amplitude and phase of spin waves [5,23]. After performing a sequence of standard canonical transformations [23–25], one arrives at the nonlinear spin-wave dynamic equation [21,23,26]

$$\frac{\partial a}{\partial t} = -i(\omega_r - \mathcal{D}_{\rm ex}\nabla^2 + \mathcal{N}_f |a|^2)a + \mathcal{T}_J(r)(a - |a|^2 a) - \mathcal{T}_\alpha(a + \kappa|a|^2 a), \tag{2}$$

where $\omega_r = \gamma\sqrt{H_{\rm int}(H_{\rm int} + 4\pi M_s \cos^2\theta_M - H_a \sin^2\theta_M)}$ is the ferromagnetic resonance frequency of the uniform mode with $H_{\rm int}$ the magnitude of the internal magnetic field given by $\mathbf{H}_{\rm int} = \mathbf{H}_{\rm ext} + H_a m_x \boldsymbol{e}_x - 4\pi M_s m_z \boldsymbol{e}_z$ and $\cos\theta_M = \mathbf{m}\cdot\boldsymbol{e}_x$, $\mathcal{T}_J(r) = \gamma a_J(r)\cos\theta_M$ characterizes the spin-wave damping or pumping rate due to the STT, $\mathcal{D}_{\rm ex} = \gamma(A_{\rm ex}/M_s)(\omega_0/\omega_H + \omega_H/\omega_0)$ is the coefficient of the exchange spin-wave dispersion with $\omega_H \equiv \gamma H_{\rm int}$, $\mathcal{T}_\alpha = \alpha_G[\omega_H + (\omega_M \cos^2\theta_M - \omega_A \sin^2\theta_M)/2]$ is the overall spin-wave damping rate with $\omega_M \equiv \gamma 4\pi M_s$ and $\omega_A \equiv \gamma H_a$, κ measures the relative spin-wave relaxation rates of nonlinear and linear processes [23], and $\mathcal{N}_f$ is the coefficient of the nonlinear spin-wave frequency shift which has been shown [23,27] to strongly depend on the out-of-plane angles of the external field and the equilibrium magnetization and may switch sign when $\mathbf{H}_{\rm ext}$ varies from in plane to perpendicular to plane, as shown in Fig. 2.

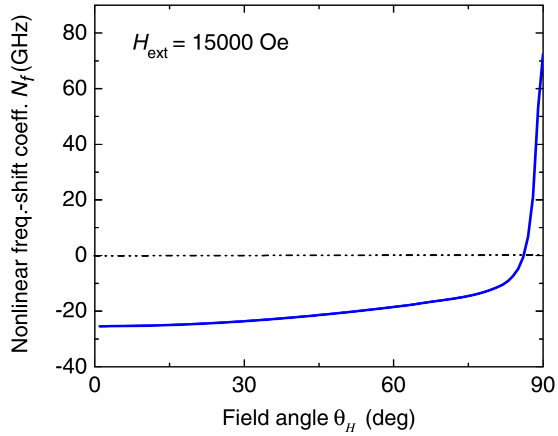

FIG. 2. Nonlinear frequency-shift coefficient $\mathcal{N}_f$ as a function of the out-of-plane field angle θ_H. Other parameters used here are $H_{\rm ext} = 15\,000$ Oe, $H_a = 500$ Oe, $M_S = 1000$ emu/cm^3, $a_J = 500$ Oe, the exchange length $l_{\rm ex} = 3$ nm [$l_{\rm ex} \equiv \sqrt{A_{\rm ex}/2\pi M_s^2}$], $R_c = 50$ nm, and radius of the free layer $R_F = 500$ nm.

Coupling between linear spin-wave modes is induced by the cubic terms $|a|^2 a$ on the rhs of Eq. (2), which originates from the four-wave processes that conserve the number of spin waves (other nonresonant-wave processes can be eliminated by the quasilinear Krasitskii transformation [24,25]). A complete set of orthonormal linear spin-wave eigenmodes $\{d_n(r,t)\}$ (with mode indices $n = 1, 2, \ldots$) can be determined by solving the linearized wave equation including the nonconservative torques

$$\frac{\partial d}{\partial t} = -i(\omega_r - \mathcal{D}_{\rm ex}\nabla^2)d - \mathcal{T}_\alpha d + \mathcal{T}_J(r)d. \tag{3}$$

The solution of Eq. (3) was obtained by Slonczewski for a perpendicularly magnetized thin film [21] and later by Slavin and Tiberkevich [26] for more general cases [see the Appendix for an outline of the solution]. We then may expand the general spin-wave mode in this basis, i.e.,

$$a(r,t) = \sum_n A_n(t)[u_n(r)e^{-i\omega_n t}], \tag{4}$$

where $A_n(t)$ are complex coefficients that describe the composition of a given spin-wave mode in terms of the linear eigenmodes and we separate the spatial and temporal components of the eigenmodes as $d_n(r,t) = u_n(r)e^{-i\omega_n t}$, where ω_n are the complex eigenfrequencies of the linearized modes. We assume that the system is operating close to, but above, the critical current for auto-oscillations so that the imaginary part of ω_n is small and can be ignored. Note that, since the experimentally observed time evolution of coupled modes [9,10,13] is usually slower than the periods of the eigenmodes $2\pi/\Re_e(\omega_n)$, it is reasonable to assume that the characteristic time scale of the variation of A_n is greater than the periods of eigenmodes of interest. By placing the expansion (4) into Eq. (2), projecting with d_i^*, and integrating the resulting equation over a time interval spanning several eigenmode periods for which the slowly varying amplitude of the ith mode $A_i(t)$ remains approximately constant [20], we arrive at the following rate equation for $A_i(t)$:

$$\frac{dA_i}{dt} = -\sum_{l,m,n}\int_0^{R_F/R_c} d^2\tilde{\mathbf{r}}[i\mathcal{N}_f + \kappa\mathcal{T}_\alpha + \mathcal{T}_J(\tilde{r})] \times u_i^*(\tilde{r})u_m^*(\tilde{r})u_l(\tilde{r})u_n(\tilde{r})A_m^* A_l A_n \delta_{\omega_i+\omega_m,\omega_l+\omega_n}, \tag{5}$$

where $\tilde{r} \equiv r/R_c$ is the dimensionless radial distance and we use the completeness relation $(2\pi)^{-1}\int dt e^{-i(\omega_n-\omega_{n'})t} = \delta_{n,n'}$.

As a minimal model to capture the essential physics underlying the coupling of linear spin-wave modes, let us focus on interactions between the two nondegenerate lowest-lying modes, namely, A_1 and A_2 with eigenenergies of ω_1 and ω_2 [assuming $\omega_1 < \omega_2$]. By imposing energy conservation on the four-wave processes, three types of term enter the mode equation: (i) the self-energy terms $A_1^*A_1A_1$ and $A_2^*A_2A_2$, (ii) the mutual energy-transfer terms $A_1^*A_1A_2$ and $A_2^*A_1A_2$, and (iii) the terms $A_m^*A_nA_2$ [with $m > n > 2$] which correspond to the four-wave processes of $a_m^*a_2^*a_na_1$. While the first two types of term give rise to the nonlinear coupling terms [7,9,20], the third type of term leads to a linear coupling between modes 1 and 2 when the higher-energy modes are thermally excited, which is usually the case for a NC STO operated at room temperature. In this case, we can replace A_m^* and A_n with thermal occupation numbers of the magnon modes m and n by taking the trace of the density matrix over magnon Fock space with m and n magnons. However, keeping in mind that the amplitude A_m of a magnon corresponds to a reduction of the total magnetization of $\sim n_B(\omega_m)g\mu_B/(M_SV) = n_B(\omega_m)/(NS)$, where V is the volume and NS the total atomic spin of the free layer, we scale the occupation numbers appropriately, i.e., $\tilde{n}_B(\omega_m) \equiv [n_B(\omega_m)+1]/(NS) \simeq n_B(\omega_m)/(NS)$ and $\tilde{n}_B(\omega_n) \equiv n_B(\omega_n)/(NS)$, respectively, where $n_B(\omega_n) = 1/(e^{\hbar\omega_n/k_BT} - 1)$. After collecting all relevant terms, we arrive at a set of rate equations describing the coupled dynamics of the two modes:

$$\begin{aligned}\frac{dA_1(t)}{dt} &= -i(\eta_{1,1}|A_1|^2 + \eta_{1,2}|A_2|^2)A_1 - \Gamma_{G,1}(P_{1,1}|A_1|^2 \\ &\quad + P_{1,2}|A_2|^2)A_1 - \Gamma_J(Q_{1,1}|A_1|^2 \\ &\quad + Q_{1,2}|A_2|^2)A_1 - R_{1,2}(T)A_2, \end{aligned} \tag{6}$$

$$\begin{aligned}\frac{dA_2(t)}{dt} &= -i(\eta_{2,1}|A_1|^2 + \eta_{2,2}|A_2|^2)A_2 - \Gamma_{G,2}(P_{2,1}|A_1|^2 \\ &\quad + P_{2,2}|A_2|^2)A_2 - \Gamma_J(Q_{2,1}|A_1|^2 + Q_{2,2}|A_2|^2)A_2 \\ &\quad - R_{2,1}(T)A_2, \end{aligned} \tag{7}$$

where $\Gamma_{G,i} = \alpha\omega_i$ (i, $j = 1$ or 2), $\Gamma_J = \gamma a_J \cos\theta_M$, $\eta_{i,j} \equiv \mathcal{N}_f \int_0^{R_F/R_c} d^2\tilde{\mathbf{r}}|u_iu_j|^2$ are the nonlinear frequency-shift coefficients, $P_{i,j} = \kappa \int_0^{R_F/R_c} d^2\tilde{\mathbf{r}}|u_iu_j|^2$ are the nonlinear damping coefficients, $Q_{i,j} = \int_0^1 d^2\tilde{\mathbf{r}}|u_iu_j|^2$ are the nonlinear coefficients associated with the STT term, and the linear mode-coupling coefficients $R_{i,j}$ are

$$\begin{aligned} R_{i,j}(\mathbf{H}_{\text{ext}}, T) = \sum_{n,m} \int_0^{R_F/R_c} & d^2\tilde{\mathbf{r}} u_i^*(\tilde{r})u_m^*(\tilde{r})u_j(\tilde{r})u_n(\tilde{r}) \\ & \times [i\mathcal{N}_f + \kappa\mathcal{T}_\alpha + \mathcal{T}_J(\tilde{r})] \\ & \times \tilde{n}_B(\omega_n)\tilde{n}_B(\omega_m)\delta_{\omega_n+\omega_j,\omega_m+\omega_i}. \end{aligned} \tag{8}$$

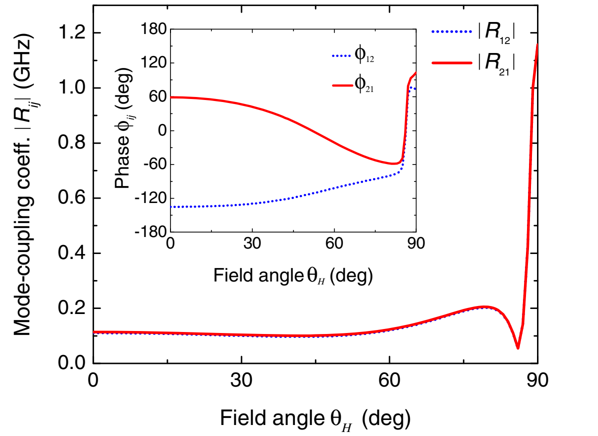

FIG. 3. Magnitude of the mode-coupling coefficients $R_{1,2}$ and $R_{2,1}$ as functions of the angle θ_H between the film plane and the external magnetic field of fixed strength 15 000 Oe at room temperature. In the inset, we show the phases of $R_{1,2}$ and $R_{2,1}$ as functions of θ_H. Other parameters used here are $\alpha = 0.05$, $M_s = 1000$ emu/cm^3, $a_J = 500$ Oe, $R_c = 50$ nm, the exchange length $l_{\text{ex}} = 3$ nm, and radius of the free layer $R_F = 500$ nm.

Note that the temperature dependence of the $R_{i,j}$ enters through the magnon thermal distribution functions $\tilde{n}_B$.

Equipped with Eq. (8), we are now in a position to investigate the dependence of the mode-coupling coefficient $R_{1,2}$ on external experimental conditions as well as intrinsic magnetic properties. In Fig. 3, we show the magnitudes and phases of the linear mode-coupling coefficients $R_{1,2}$ and $R_{2,1}$ as functions of the out-of-plane field angle θ_H. We note that the magnitudes of coupling coefficients are about subgigahertz for an applied external field of 15 000 Oe. This justifies our assumption that the time evolution of $A_n(t)$ ($n = 1, 2$) is slow compared to the fast dynamics of the magnetization. Also, the magnitude of the coefficients $R_{i,j}$ approaches a global minimum at a field angle of $\theta_H = 86°$, which coincides with the field angle at which the nonlinear spin-wave frequency-shift coefficient $\mathcal{N}_f$ changes sign, as demonstrated in Fig. 2. In addition, the phase difference increases as the field angle moves away from the zero-crossing point of the nonlinear frequency shift. The link between the linear mode coupling and the nonlinear spin-wave frequency shift may suggest a way to control and manipulate the mode coupling.

In Fig. 4, we show the temperature dependence of the mode-coupling coefficients $R_{1,2}$ and $R_{2,1}$ for $H_{\text{ext}} = 15\,000$ Oe at several out-of-plane field angles. We see that the magnitudes of both $R_{1,2}$ and $R_{2,1}$ increase algebraically with the temperature. This can be understood by recalling that the linear mode coupling stems from interactions between the two dominant modes and thermally occupied magnons via the four-magnon scattering processes. The density of thermal magnons increases at elevated temperatures, which gives rise to more scattering space that contributes to the linear mode coupling. This temperature

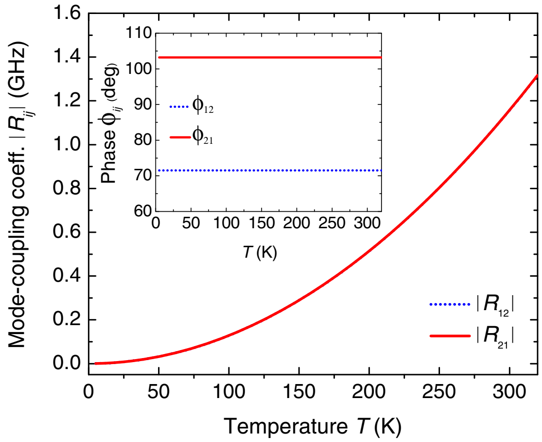

FIG. 4. Magnitude of the mode-coupling coefficients $R_{1,2}$ and $R_{2,1}$ as functions of temperature T with an external magnetic field H_{ext} of 15 000 Oe applied perpendicular to the plane of the layer. In the inset, we show the phase of $R_{1,2}$ and $R_{2,1}$ as functions of T. Other parameters: $\alpha_G = 0.05$, $M_S = 1000\ \text{emu/cm}^3$, $a_J = 500$ Oe, $R_c = 50$ nm, the exchange length $l_{\text{ex}} = 3$ nm, and radius of the free layer $R_F = 500$ nm.

dependence, as we show later, implies that the temperature alone can change the manifold of the system's dynamics and leads to thermally induced mode hopping [17] consistent with experimental observations [10]. The phases of the coupling coefficients, however, are insensitive to the temperature, as shown in the inset in Fig. 4, since we implicitly make the random phase approximation whereby the thermal magnons of different wave vectors are taken to be incoherent.

III. PHASE PORTRAIT OF THE MODE EQUATIONS

Although the energy of an individual mode varies instantaneously through pumping and damping, we may assume that the total energy of the two dominant modes 1 and 2 is approximately conserved on time scales much longer than the periods of the eigenmodes, i.e.,

$$\omega_1|A_1|^2 + \omega_2|A_2|^2 = \omega, \tag{9}$$

where ω is a constant, the value of which indicates the total energy in the two-mode subsystem. The substitution of $A_i(t) = K_i(t)e^{i\phi_i(t)}$ $[i = 1,\ 2]$ into Eq. (9) immediately reveals the relation between the amplitudes of the two modes, which can be captured by the following transformation [15]: $\sqrt{\omega_1}K_1 = \sqrt{\omega}\cos[(\theta/2) + (\pi/4)]$ and $\sqrt{\omega_2}K_2 = \sqrt{\omega}\sin[(\theta/2) + (\pi/4)]$, where the variable θ characterizes the relative magnitude of the two mode amplitudes. Placing these transformations into the mode equations (6) and (7) and separating the real and imaginary parts of the resulting equations, we arrive at a set of coupled dynamic equations for two real variables, i.e.,

$$\begin{aligned}\dot{\theta} = {} & \omega\cos\theta\left[(\Gamma_{G,1}P_{1,1} - \Gamma_{G,2}P_{2,1})\left(\frac{1-\sin\theta}{2\omega_1}\right) - (\Gamma_{G,2}P_{2,2} - \Gamma_{G,1}P_{1,2})\left(\frac{1+\sin\theta}{2\omega_2}\right)\right] \\ & + \omega\Gamma_J\cos\theta\left[(Q_{1,1} - Q_{2,1})\left(\frac{1-\sin\theta}{2\omega_1}\right) - (Q_{2,2} - Q_{1,2})\left(\frac{1+\sin\theta}{2\omega_2}\right)\right] \\ & + \mathfrak{R}_e(R_{2,1}e^{-i\psi})\sqrt{\frac{\omega_2}{\omega_1}}(1-\sin\theta) - \mathfrak{R}_e(R_{1,2}e^{i\psi})\sqrt{\frac{\omega_1}{\omega_2}}(1+\sin\theta)\end{aligned} \tag{10}$$

and

$$\begin{aligned}\dot{\psi} = {} & \omega\left[(\eta_{1,1} - \eta_{2,1})\left(\frac{1-\sin\theta}{2\omega_1}\right) - (\eta_{2,2} - \eta_{1,2})\left(\frac{1+\sin\theta}{2\omega_2}\right)\right] \\ & + \mathfrak{I}_m(R_{2,1}e^{-i\psi})\ \sec\theta\sqrt{\frac{\omega_2}{\omega_1}}(1-\sin\theta) \\ & - \mathfrak{I}_m(R_{1,2}e^{i\psi})\ \sec\theta\sqrt{\frac{\omega_1}{\omega_2}}(1+\sin\theta),\end{aligned} \tag{11}$$

where $\psi \equiv \phi_2 - \phi_1$ is the phase difference of the two modes. As we can see, the original mode equations, which involve four independent dynamical variables, have been mapped onto a two-dimensional phase space, similar to those describing the dynamics of a ring laser with backscattering [15,16].

In a previous work [17], a similar set of the coupled effective mode equations is solved for a given external field and temperature, with the various coefficients being treated as phenomenological parameters. Notably, the coefficients of the linear coupling terms are assumed to be complex conjugates, which is manifestly *not* generally true (see Figs. 3 and 4). Now that we have derived these coefficients as functions of the external field and temperature, we are in a position to further investigate the evolution of the two modes in the phase space spanned by θ and ψ for varying field angles and temperatures. We note that, because the system of equations (10) and (11) is invariant under the transformations $\theta \to \pm\pi - \theta$ and $\psi \to \psi \pm \pi$, in principle, it suffices to show the phase space for $-(\pi/2) < \theta < (\pi/2)$; however, we choose to show the phase space in the extended zone of $-\pi < \theta < \pi$ in order to avoid a confusing overlay of trajectories

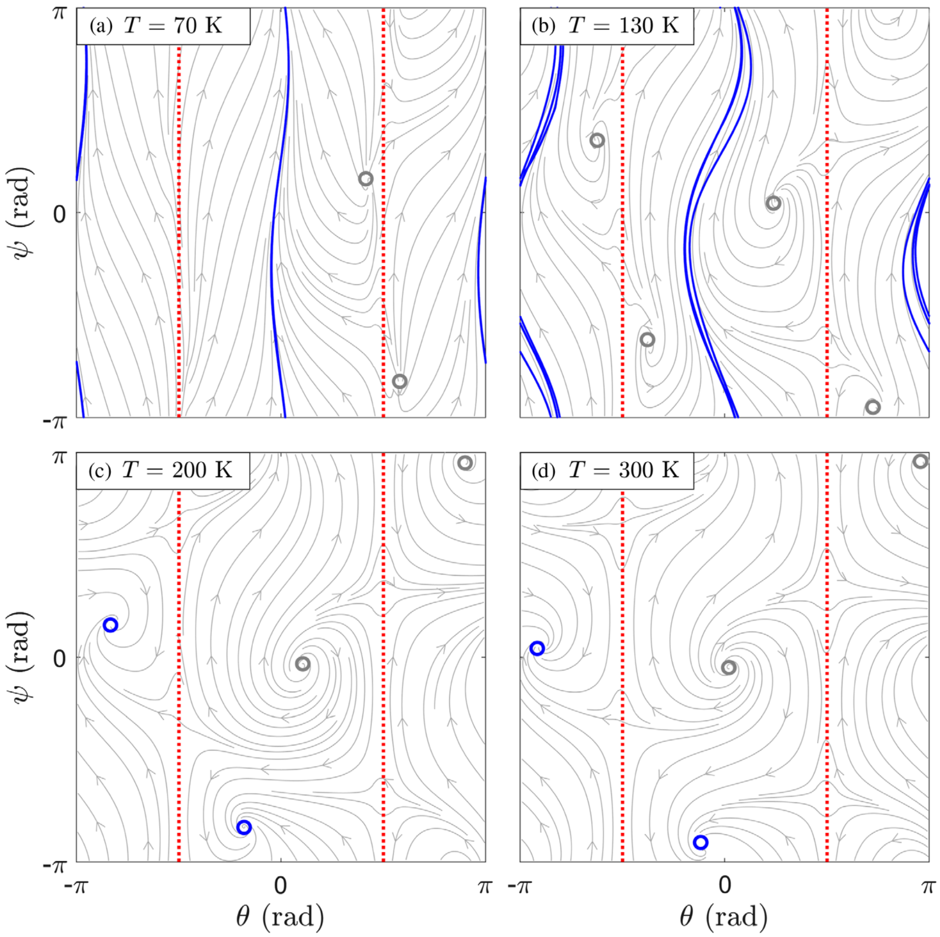

FIG. 5. Portrait of the dynamics of two coupled modes in the phase space spanned by θ and ψ for an external field of 15 000 Oe and $\theta_H = 82°$ at (a) $T = 70$ K, (b) $T = 130$ K, (c) $T = 200$ K, and (d) $T = 300$ K. The vertical red dotted lines denote the singularities at $\theta = \pm(\pi/2)$. As the mode-coupling magnitude increases with the temperature, the trajectories (blue lines) established by unstable fixed points (gray circles) transition into stable fixed points (blue circles). In all cases, the features are even indicating in-phase and out-of-phase synchronized modes.

corresponding to in-phase and out-of-phase solutions with crossing of trajectories, which is prohibited by the uniqueness of solutions for dynamical systems that evolve smoothly. Note that this extended scheme depicts the singularities at $\theta = \pm(\pi/2)$ given by Eq. (11).

In Fig. 5, we show the phase portraits of mode dynamics for $\omega = 1$ GHz at several different temperatures with a given external field of magnitude 15 000 Oe and angle $\theta_H = 82°$. In this case, the coupling phase is constant and only the magnitude increases with the temperature, similar to the perpendicular-to-plane case shown in Fig. 4. Well below room temperature ($T = 300$ K), pairs of unstable fixed points (solid gray circles) are present as shown in Figs. 5(a) and 5(b), which are accompanied by steady-state trajectories (solid blue lines) representing the coexistence of the two modes with a periodic mutual energy transfer due to the mode coupling. As the temperature increases, some of the unstable fixed points are converted into stable ones due to the increased strength of the linear mode coupling [as shown in Fig. 5(c)]. When the temperature is further increased, the linear mode coupling dominates and the fixed points have to approach $\theta = \pm\pi$ or $\theta = 0$, as indicated by Fig. 5(d).

Physically, stable fixed points correspond to phase-locked or synchronized modes; i.e., the differences in both the phase and energy of the two modes remain constant in time. The existence of equal numbers of stable and unstable fixed points across the singularities (red dotted lines) is consistent with an in-phase–out-of-phase synchronization. These results demonstrate that the phase portrait of the multimode dynamics in a NC STO can be strongly affected by the temperature and can lead to mode transitions, in agreement with experimental observations of temperature-dependent mode transitions above room temperature [10]. We note that, in the calculation of the phase portraits, the temperature dependence enters only through the linear mode-coupling coefficients $R_{i,j}$ in Eqs. (10) and (11). The inclusion of the temperature as a stochastic field merely blurs the phase portraits and potentially leads to mode transitions across saddle points on the stable manifolds, leading to mode hopping [9,17], but does not change the orbits or manifolds themselves.

More complex behaviors are found when the external field angle θ_H is varied at a fixed temperature $T = 200$ K (as shown in Fig. 6), in which case both the magnitude and phase of the linear mode-coupling coefficients $R_{i,j}$ vary with θ_H. We consider four regimes as the field angle increases: (i) weak coupling magnitude and large phase difference, (ii) weak coupling magnitude and small phase difference; (iii) local coupling magnitude maximum and small phase difference; and (iv) strong coupling magnitude

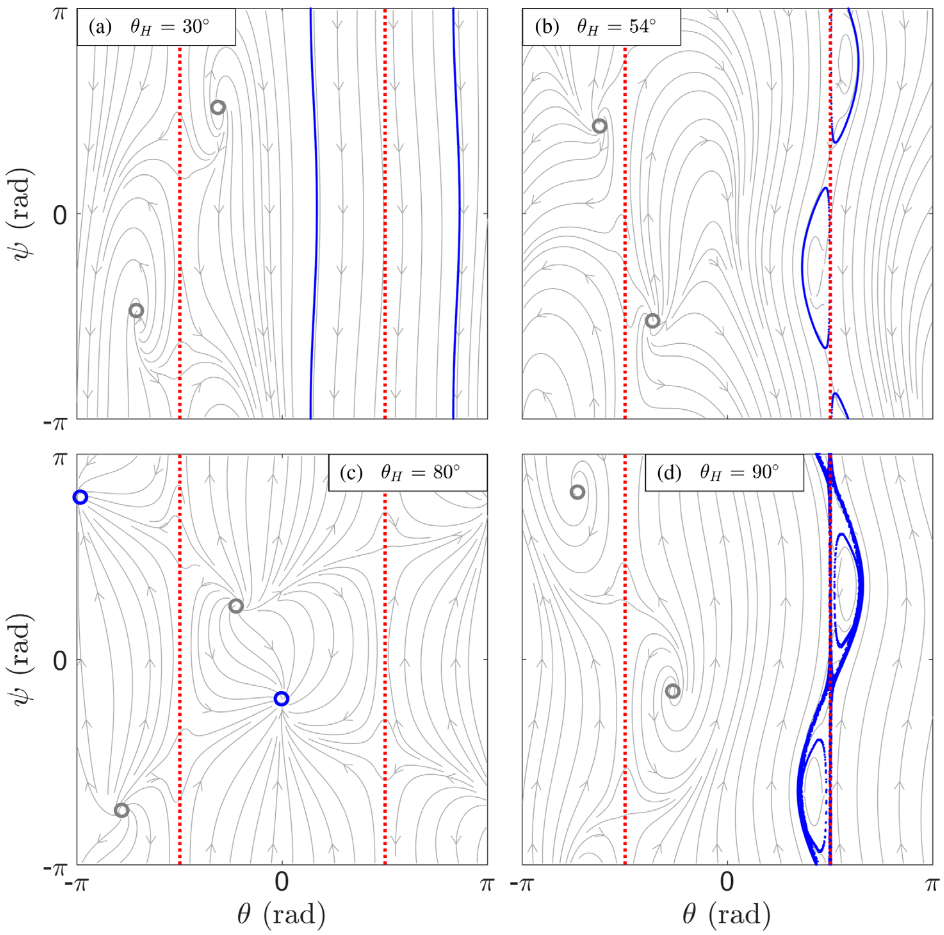

FIG. 6. Portrait of the dynamics of two coupled modes in the phase space spanned by θ and ψ for an external field of 15 000 Oe and $T = 200$ K at (a) $\theta_H = 30°$, (b) $\theta_H = 54°$, (c) $\theta_H = 80°$, and (d) $\theta_H = 90°$. (a) Unstable fixed points (gray circles) define trajectories (blue lines) for small external field angles. (b) Closed orbits (blue) are observed when the coupling angles are similar. (c) Stable and unstable fixed points (blue and gray circles) are observed at the local coupling strength maximum and identical coupling phase angles. (d) Closed orbits and heterocliniclike orbits are observed at the high-symmetry condition of a perpendicularly magnetized sample.

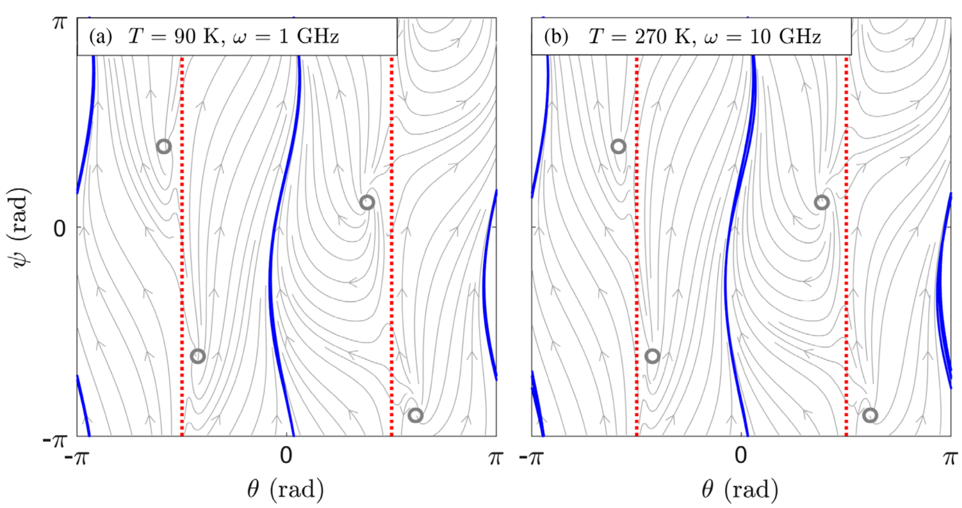

FIG. 7. Portrait of the dynamics of two coupled modes in the phase space spanned by θ and ψ for an external field of 15 000 Oe and $\theta_H = 82°$ at (a) $T = 90$ K, $\omega = 1$ GHz and (b) $T = 270$ K, $\omega = 10$ GHz. Both phase portraits are equivalent.

and identical phases. Exemplary phase portraits of these regimes are shown in Fig. 6 as the angle is varied from in plane to perpendicular to plane. For case (i) [Fig. 6(a)], the phase portrait exhibits two unstable fixed points (spirals) and stable steady-state trajectories, similar to the phase portraits well below room temperature as shown in Fig. 5(a). For case (ii) shown in Fig. 6(b), the trajectories get pulled around to form the large elliptical closed orbits which imply the self-sustained periodic oscillation of the coupled subsystem. For case (iii) [Fig. 6(c)], the two closed orbits collapse to two stable fixed points as the system reaches a local maximum of linear mode coupling strength (see Fig. 3). Finally, for (iv), the phase portrait is again dominated by closed orbits [Fig. 6 (d)] accompanied by heterocliniclike orbits and chaotic dynamics near the singular line $\theta = \pi/2$. This observation is consistent

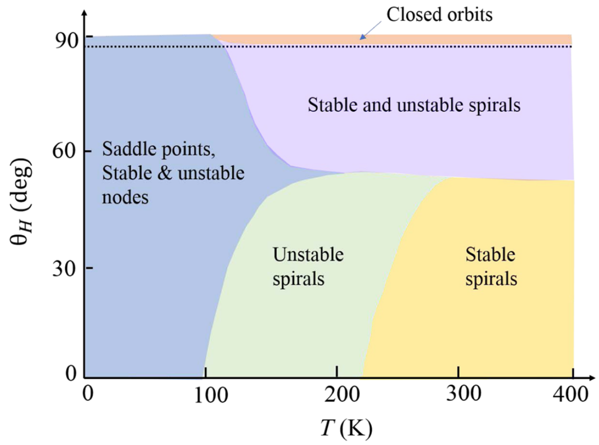

FIG. 8. Phase diagram of coupled mode dynamics as a function of the temperature and field angle of the external magnetic field with a fixed magnitude of 15 000 Oe. Closed orbits and several different types of fixed point are shown, such as saddle points, nodes, spirals, etc., and their stability changes across the phase boundaries. The horizontal black dotted line denotes the field angle of 86° (i.e., the zero-crossing point of the nonlinear frequency shift), above which large closed orbits appear at elevated temperatures ($T > 100$ K) as the strength of the linear mode coupling grows rapidly.

with the poor spectral content of STT-driven excitations in perpendicularly magnetized STOs [4] despite the fact that such a high-symmetry case theoretically favors a Slonczewski mode in a single-mode approximation.

In addition to the field and temperature dependence of the coupled mode dynamics, another observation is that increasing (decreasing) the amount of energy in the two-mode subsystem (characterized by ω) is equivalent to reducing (enhancing) the strength of the linear coupling coefficients $R_{i,j}$. This can be seen if one divides both sides of Eqs. (10) and (11) by ω, and the resulting equations indicate that the steady-state solutions of the system rely only on the ratio $|R_{i,j}|/\omega$. To illustrate this effect, we show in Fig. 7 the nearly identical phase portraits at a fixed field angle of $\theta_H = 82°$ for two different sets of parameters: (a) temperatures and (a) $T = 90$ K, $\omega = 1$ GHz and (b) $T = 270$ K, $\omega = 10$ GHz. This is consistent with the fact that the strength of linear mode-coupling coefficient for $\theta_H = 82°$ at $T = 270$ K is about 10 times as large as that for $T = 90$ K, according to Fig. 4.

Last, in Fig. 8, we show a schematic phase diagram of the dynamic behavior of the coupled mode system as a function of the field angle and temperature, which depicts how changing these control parameters alters the dynamical landscape.

IV. SUMMARY AND CONCLUSIONS

We theoretically investigate the coupled dynamics of linear spin-wave eigenmodes in NC STOs using a previously derived multimode theory [9,17,20]. For a simple but experimentally relevant geometry in which the external magnetic field and both equilibrium magnetizations of the free and fixed layers are coplanar, we derive the rate equations that govern the slow dynamics of a subsystem involving several dominant modes, as a generalization of the single-mode STO theory proposed earlier by Slavin and Tiberkevich [5,23,26]. In this particular geometry, we could explicitly calculate the mode-coupling coefficients in the multimode theory and transform the system of equations for two dominant modes into an effective two-dimensional driven dynamic system. This allows us to explore the effect of an external field and the temperature on the phase portraits of the system and to draw several conclusions about the dynamics of the system. First of all, there is an intimate relation between the nonlinear frequency shift and the linear mode coupling [Eq. (8)]. This leads to a minimum in the magnitudes of the mode-coupling coefficients when the nonlinear frequency shift is zero, concomitant with a steep change in the phase shift between them. There are profound consequences in the resulting dynamics and phase portraits as the mode-coupling coefficients go through their minimum. The phase portrait of the subdynamical system changes rapidly, exhibiting closed orbits and a set of different types of fixed point as well as the change of their stabilities. This is consistent with and explains the observed behavior in STOs [4]. Second, our work explains, through the temperature dependence of the mode-coupling coefficients, how the temperature alone can drive the dynamics of the system from one set of orbits and fixed points to another. This is consistent with experimental observations [10] that to the best of our knowledge have eluded explanation; a thermal stochastic field (not included here) only perturbs the orbits about the underlying manifold. A stochastic field is, however, necessary to induce mode hopping [9,17] over saddle points separating orbits. Among other things, our analysis reveals that increasing the power in the two-mode subsystem may effectively suppress the linear mode coupling, as the system becomes less perturbed by the interaction between the modes.

Last, we stress that the multimode theory that we derive here is based on the expansion of general solutions of modes in terms of the linear combination of eigenmodes, which are propagating spin-wave modes in the present case, and hence is not applicable for describing the coupled magnetodynamics involving a localized bullet mode [14,26].

ACKNOWLEDGMENTS

The authors are grateful to Y. C. Li for helpful discussions. Work by S. S.-L. Z. is supported by NSF Grant No. DMR-1406568 and partly by Department of Energy, Office of Science, Materials Sciences and Engineering Division through Materials Theory Institute. E. I. acknowledges support from the Swedish Research Council, Reg. No. 637-2014-6863. Work by O. H. is supported by the U.S. Department of Energy (DOE), Office of Science, Division of Materials Sciences and Engineering, and O. H.

gratefully acknowledges the computing resources provided on Blues and Fusion, high-performance computing clusters operated by the Laboratory Computing Resource Center at Argonne National Laboratory.

APPENDIX: LINEAR SPIN-WAVE MODE IN NC STO

In this Appendix, we outline the derivation of the profiles of the linear spin-wave mode by solving Eq. (3) given in the main text. Separating the time and spatial variables of the wave-function profile, i.e.,

$$d(\tilde{r},t) = Ce^{-i\omega t}\nu(\tilde{r}), \tag{A1}$$

where C is the normalization coefficient to be determined by boundary conditions and $\tilde{r} \equiv r/R_c$ is the dimensionless radial distance. Placing Eq. (A1) in Eq. (3), we arrive at a zeroth-order Bessel equation for the spatial part of the wave function:

$$\tilde{r}^2\frac{d^2}{d\tilde{r}^2}\nu(\tilde{r}) + \tilde{r}\frac{d}{d\tilde{r}}\nu(\tilde{r}) + (\tilde{\omega} - \tilde{\omega}_r + i\tilde{\Gamma}_\alpha - i\tilde{\Gamma}_J)\tilde{r}^2\nu(\tilde{r}) = 0, \tag{A2}$$

where $\tilde{\omega}_r \equiv \omega_r/(D_{\rm ex}/R_c^2)$, $\tilde{\omega} \equiv \omega/(D_{\rm ex}/R_c^2)$, $\tilde{\Gamma}_\alpha \equiv \Gamma_\alpha/(D_{\rm ex}/R_c^2)$, and $\tilde{\Gamma}_J = \Gamma_J/(D_{\rm ex}/R_c^2)$. The general solution for $\tilde{r} \leq 1$ reads

$$\nu_<(\tilde{r}) = C_1J_0(\kappa_<\tilde{r}), \tag{A3}$$

where J_0 is the zeroth-order Bessel function with

$$\kappa_<^2 = \tilde{\omega} - \tilde{\omega}_r + i\tilde{\Gamma}_\alpha - i\tilde{\Gamma}_J. \tag{A4}$$

For $\tilde{r} > 1$, we should have an outgoing wave, so the Hankel function of the first kind is chosen, i.e.,

$$\nu_>(\tilde{r}) = C_2H_0^{(1)}(\kappa_>\tilde{r}), \tag{A5}$$

where

$$\kappa_>^2 = \tilde{\omega} - \tilde{\omega}_r + i\tilde{\Gamma}_\alpha. \tag{A6}$$

The coefficients C_1 and C_2 are determined by the matching boundary condition as well as the normalization condition, i.e.,

$$C_1J_0(\kappa_<) = C_2H_0^{(1)}(\kappa_>), \tag{A7}$$

and

$$\int_0^{R_F/R_c} d\tilde{r}\,\tilde{r}\,|d(\tilde{r})|^2 = 1. \tag{A8}$$

Explicitly, we have

$$|C_1|^2 = \frac{|H_0^{(1)}(\kappa_>)|^2}{|H_0^{(1)}(\kappa_>)|^2\int_0^1 d\tilde{r}\,\tilde{r}\,|d(\tilde{r})|^2 + |J_0(\kappa_<)|^2\int_1^{R_F/R_c} d\tilde{r}\,\tilde{r}\,|d(\tilde{r})|^2}, \tag{A9}$$

and

$$|C_1|^2 = \frac{|J_0(\kappa_<)|^2}{|H_0^{(1)}(\kappa_>)|^2\int_0^1 d\tilde{r}\,\tilde{r}\,|d(\tilde{r})|^2 + |J_0(\kappa_<)|^2\int_1^{R_F/R_c} d\tilde{r}\,\tilde{r}\,|d(\tilde{r})|^2}. \tag{A10}$$

By matching the wave functions and their derivatives at $\tilde{r} = 1$, we find a transcendental equation

$$\frac{\kappa_<J_1(\kappa_<)}{J_0(\kappa_<)} = \frac{\kappa_>H_1^{(1)}(\kappa_>)}{H_0^{(1)}(\kappa_>)}, \tag{A11}$$

where we use the recurrence relation $dZ_0(x)/dx = -Z_1(x)$ with Z denoting J or $H^{(1)}$. Solving this equation, we can obtain the eigenmodes for a given current density. There are infinitely many solutions corresponding to the excited spin-wave modes with different wave vectors (associated with the number of nodes n in the current flowing region). The spin-wave frequency in the ultrathin limit ($k_nd \ll 1$) can be expressed as [28–30]

$$\omega_n = \sqrt{(\omega_H + D_{\rm ex}k_n^2)(\omega_H + D_{\rm ex}k_n^2 + \omega_M\cos^2\theta_M - \omega_A\sin^2\theta_M)}. \tag{A12}$$

By solving Eq. (A11), we find the wave vectors of the two lowest spin-wave modes are

$$k_1 = 1.76/R_c \quad \text{and} \quad k_2 = 4.61/R_c. \tag{A13}$$

As indicated by Eqs. (A4) and (A6), the wavelengths of excited spin waves, in general, depend on both the damping and current; in the small damping limit, we recover Slonczewski's result [21] of $k_1 = 1.19/R_c$ and $k_2 = 4.5/R_c$.

[1] J. C. Slonczewski, Current-driven excitation of magnetic multilayers, J. Magn. Magn. Mater. **159**, L1 (1996).

[2] L. Berger, Emission of spin waves by a magnetic multilayer traversed by a current, Phys. Rev. B **54**, 9353 (1996).

[3] T. J. Silva and W. H. Rippard, Developments in nano-oscillators based upon spin-transfer point-contact devices, J. Magn. Magn. Mater. **320**, 1260 (2008).

[4] R. K. Dumas, S. R. Sani, S. M. Mohseni, E. Iacocca, Y. Pogoryelov, P. K. Muduli, S. Chung, P. Dürrenfeld, and J. Åkerman, Recent advances in nanocontact spin-torque oscillators, IEEE Trans. Magn. **50**, 1 (2014).

[5] A. Slavin and V. Tiberkevich, Nonlinear auto-oscillator theory of microwave generation by spin-polarized current, IEEE Trans. Magn. **45**, 1875 (2009).

[6] G. Bertotti, C. Serpico, I. D. Mayergoyz, A. Magni, M. d'Aquino, and R. Bonin, Magnetization Switching and Microwave Oscillations in Nanomagnets Driven by Spin-Polarized Currents, Phys. Rev. Lett. **94**, 127206 (2005).

[7] F. M. de Aguiar, A. Azevedo, and S. M. Rezende, Theory of a two-mode spin torque nanooscillator, Phys. Rev. B **75**, 132404 (2007).

[8] I. N. Krivorotov, N. C. Emley, R. A. Buhrman, and D. C. Ralph, Time-domain studies of very-large-angle magnetization dynamics excited by spin transfer torques, Phys. Rev. B **77**, 054440 (2008).

[9] P. K. Muduli, O. G. Heinonen, and J. Åkerman, Decoherence and Mode Hopping in a Magnetic Tunnel Junction Based Spin Torque Oscillator, Phys. Rev. Lett. **108**, 207203 (2012).

[10] P. K. Muduli, O. G. Heinonen, and J. Åkerman, Temperature dependence of linewidth in nanocontact based spin torque oscillators: Effect of multiple oscillatory modes, Phys. Rev. B **86**, 174408 (2012).

[11] S. Bonetti, V. Tiberkevich, G. Consolo, G. Finocchio, P. Muduli, F. Mancoff, A. Slavin, and J. Åkerman, Experimental Evidence of Self-Localized and Propagating Spin Wave Modes in Obliquely Magnetized Current-Driven Nanocontacts, Phys. Rev. Lett. **105**, 217204 (2010).

[12] S. Bonetti, V. Puliafito, G. Consolo, V. S. Tiberkevich, A. N. Slavin, and J. Åkerman, Power and linewidth of propagating and localized modes in nanocontact spin-torque oscillators, Phys. Rev. B **85**, 174427 (2012).

[13] R. K. Dumas, E. Iacocca, S. Bonetti, S. R. Sani, S. M. Mohseni, A. Eklund, J. Persson, O. Heinonen, and J. Åkerman, Spin-Wave-Mode Coexistence on the Nanoscale: A Consequence of the Oersted-Field-Induced Asymmetric Energy Landscape, Phys. Rev. Lett. **110**, 257202 (2013).

[14] E. Iacocca, P. Dürrenfeld, O. Heinonen, J. Åkerman, and R. K. Dumas, Mode-coupling mechanisms in nanocontact spin-torque oscillators, Phys. Rev. B **91**, 104405 (2015).

[15] S. Beri, L. Gelens, M. Mestre, G. Van der Sande, G. Verschaffelt, G. Scirè, G. Mezosi, M. Sorel, and J. Danckaert, Topological Insight into the Non-Arrhenius Mode Hopping of Semiconductor Ring Lasers, Phys. Rev. Lett. **101**, 093903 (2008).

[16] G. van der Sande, L. Gelens, P. Tassin, J. Scirè, and A. Danckaert, J. Phys. B **41**, 095402 (2008).

[17] E. Iacocca, O. Heinonen, P. K. Muduli, and J. Åkerman, Generation linewidth of mode-hopping spin torque oscillators, Phys. Rev. B **89**, 054402 (2014).

[18] N. Sharma, P. Dürrenfeld, E. Iacocca, O. Heinonen, and J. Åkerman, Mode-hopping mechanism generating colored noise in a magnetic tunnel junction based spin torque oscillator, Appl. Phys. Lett. **105**, 132404 (2014).

[19] A. Eklund, S. Bonetti, S. R. Sani, S. Majid Mohseni, J. Persson, S. Chung, S. Amir Hossein Banuazizi, E. Iacocca, M. Östling, J. Åkerman, and B. Gunnar Malm, Dependence of the colored frequency noise in spin torque oscillators on current and magnetic field, Appl. Phys. Lett. **104**, 092405 (2014).

[20] S. S.-L. Zhang, Y. Zhou, D. Li, and O. Heinonen, Mode coupling in spin torque oscillators, J. Magn. Magn. Mater. **414**, 227 (2016).

[21] J. C. Slonczewski, Excitation of spin waves by an electric current, J. Magn. Magn. Mater. **195**, L261 (1999).

[22] We note that, in experiments, the application of a large external field slightly tilts the magnetization of the fixed layer out of plane. We ignore such out-of-plane components, as they are small and primarily lead only to a small renormalization of the STT. Similarly, we are ignoring fieldlike STT, as it would slightly renormalize the external magnetic field.

[23] A. Slavin and V. Tiberkevich, Excitation of spin waves by spin-polarized current in magnetic nano-structures, IEEE Trans. Magn. **44**, 1916 (2008).

[24] V. P. Krasitskii, Canonical transformation in a theory of weakly nonlinear waves with a nondecay dispersion law, Sov. Phys. JETP **71**, 921 (1990).

[25] V. S. L'vov, *Wave Turbulence Under Parametric Excitations: Applications to Magnets* (Springer, Berlin, 1994).

[26] A. Slavin and V. Tiberkevich, Spin Wave Mode Excited by Spin-Polarized Current in a Magnetic Nanocontact is a Standing Self-Localized Wave Bullet, Phys. Rev. Lett. **95**, 237201 (2005).

[27] P. Krivosik and C. E. Patton, Hamiltonian formulation of nonlinear spin-wave dynamics: Theory and applications, Phys. Rev. B **82**, 184428 (2010).

[28] K. J. Harte, Theory of magnetization ripple in ferromagnetic films, J. Appl. Phys. **39**, 1503 (1968).

[29] R. Arias and D. L. Mills, Extrinsic contributions to the ferromagnetic resonance response of ultrathin films, Phys. Rev. B **60**, 7395 (1999).

[30] R. D. McMichael, M. D. Stiles, P. J. Chen, and W. F. Egelhoff, Ferromagnetic resonance linewidth in thin films coupled to nio, J. Appl. Phys. **83**, 7037 (1998).